Computational Materials Science 171 (2020) 109232

Contents lists available at ScienceDirect

Computational Materials Science

journal homepage: www.elsevier.com/locate/commatsci

A novel two-dimensional mechanical metamaterial with negative Poisson's ratio

Hui Wang[a,*], Yuxuan Zhang[a], Wanqing Lin[a], Qing-Hua Qin[b,*]

[a] College of Civil Engineering, Henan University of Technology, Zhengzhou 450001, China

[b] Research School of Electrical, Energy and Materials Engineering, Australian National University, ACT 2601, Australia

ARTICLE INFO

Keywords:
Auxetic material
Microstructure
Negative Poisson's ratio
Tensile test
Finite element analysis

ABSTRACT

Artificial auxetic materials with negative Poisson's ratio enable distinctive elastic response in the direction orthogonal to the loaded direction, i.e. shrinking when compressed and expanding when stretched, compared to conventional materials. Such distinctive mechanical characteristic makes auxetic materials unique in practice. Current studies in this aspect focus mainly on the realization of beam-dominated microstructures such as re-entrant and chiral lattices and of cellular microstructures with orthogonal elliptical hole pattern. In this study, a novel two-dimensional auxetic microstructure is designed by introducing peanut-shaped holes in solid bulk matrix. Compared to the microstructure with elliptical hole pattern, the present design can produce slightly larger negative Poisson's ratio and achieve significantly lower stress level. The samples consisting of a number of centimeter-scale unit cells with the peanut-shaped holes are fabricated efficiently via additive manufacturing technique. Experiment and finite element simulation of tensile test are carried out on the specific sample to demonstrate the auxetic effect of the present design and simultaneously verify the computational model. Finally, effects of some parameters on Poisson's ratio, which may control the auxetic behavior of the present microstructure, are discussed for better understanding deformation mechanism of the proposed auxetic material.

1. Introduction

The concept of metamaterials with specially designed artificial microstructure made by additive manufacturing technology has recently received more and more attention because of its unconventional physical properties that are previously inaccessible in conventional materials [1–4]. With these man-made metamaterials, engineering materials with various properties have been developed including negative Poisson's ratio (auxetic properties) [5–11], zero/negative thermal expansion materials [12,13], cloaking materials [14,15], phononic materials [16–19], twistable materials [20,21], and materials with vibration absorption [22,23]. Among these examples, mechanical consistence between longitudinal and orthogonal transverse elastic deformations has been achieved in two-dimensional (2D) and three-dimensional (3D) cellular metamaterials with well-designed cellular topologies [24], i.e. re-entrant shape (Fig. 1a), chiral shape (Fig. 1b) and elliptical hole shape (Fig. 1c) [5–11]. In the static case, such mechanical consistence is conflicted to the fact that a conventional elastic solid cannot expand or shrink laterally when stretched or compressed longitudinally (Fig. 1d) [6,25,26]. It has been revealed that the auxetic behavior of a material can be regarded as a consequence of rotation of elastic cell when it is subjected to a compressive or tensile load [5]. Therefore, auxetic structures with negative Poisson's ratio are beneficial to enhancing shear rigidity, indentation resistance, toughness, energy dissipation ability and acoustic absorption ability in various applications [27–31].

However, the current re-entrant and chiral metamaterials [9,10] with negative Poisson's ratio are generally designed to have beam-dominated microstructures with bending dominated topologies. As a result, they are known to have low macroscopic stiffness, high flexibility, and high porosity. More seriously, joints with sharp corners in the re-entrant and chiral auxetic structures could lead to high stress concentration [32]. As an alternative to the beam-dominated auxetic microstructures, the orthogonal elliptical hole pattern in solid material was revealed to be beneficial in achieving controllable auxetic response. However, the elliptical hole usually leads to high stress level too. In order to achieve the balance of stiffness and flexibility, and meanwhile possess smoothed boundary and controllable porosity, in this study, a new two-dimensional elastic cellular metamaterial with a negative Poisson's ratio is designed, fabricated, and characterized. Inspired by the research reported in literature [11,33,34], the present microstructure is designed by introducing a square array of mutually orthogonal peanut-shaped holes in a 2D solid sheet characterized with

* Corresponding authors.
E-mail addresses: huiwang@haut.edu.cn (H. Wang), qinghua.qin@anu.edu.au (Q.-H. Qin).

https://doi.org/10.1016/j.commatsci.2019.109232
Received 11 July 2019; Received in revised form 24 August 2019; Accepted 26 August 2019

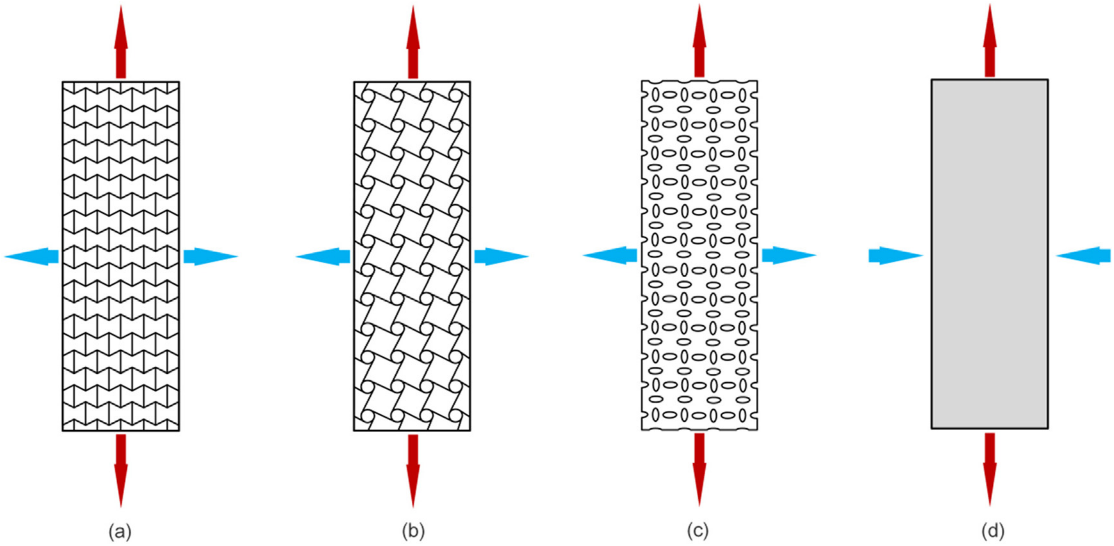

Fig. 1. Different transverse mechanical responses (blue arrow) for (a) auxetic material with re-entrant microstructure, (b) auxetic material with chiral microstructure, (c) auxetic material with elliptical holes and (d) conventional elastic solid material when stretched (red arrow).

desired porosity. The new design is geometrically distinct from previously established beam-dominated topologies and tunable elastic topologies with mutually orthogonal elliptical holes of mechanical metamaterials. Comparisons of Poisson's ratio and stress level are made to illustrate advantages of the present design over the existing design with elliptical holes. The deformation mechanism of the new configuration is also revealed. Then, the characterization of mechanical properties of parametric cell is conducted by means of experiment and numerical method for further exploring its auxetic performance.

2. Modelling and deformation mechanism

2.1. Unit cell design

It is well known that both the base material and cell topologies can control the mechanical properties of cellular auxetic materials [10]. In this study, the peanut-shaped hole shown in Fig. 2a is generated to cut arbitrary base material to form a symmetric metamaterial unit cell, as shown in Fig. 2b. In Fig. 2a, the geometry shape of peanut hole is characterized by two small circles of radius r and two tangent large circles of radius R. Then, the centroid distance s of the two large circles is determined by

$$s = \sqrt{4(r+R)^2 - d^2} = 2\sqrt{(r+R)^2 - \frac{d^2}{4}} \tag{1}$$

where d is the centroid distance of the two small circles.

With the established peanut-shaped hole, the symmetric metamaterial unit cell can be designed by cutting the base material with nine holes, as indicated in Fig. 2b. The lengths of the ligaments separating neighboring holes are denoted as m_1 and m_2 in the x and y directions, respectively. Then, the side lengths L_1 and L_2 of the unit cell can be determined. Here, for the sake of simplicity, it is assumed that $m_1 = m_2 = m$, thus the unit cell is a square with side length $L_1 = L_2 = L$, which can be calculated using the following expression

$$L = d + 2r + s - 2R + 2m \tag{2}$$

from which the void porosity of the unit cell can be evaluated by

$$\phi = \frac{4A}{L^2} \tag{3}$$

where A is the area of each peanut-shaped hole:

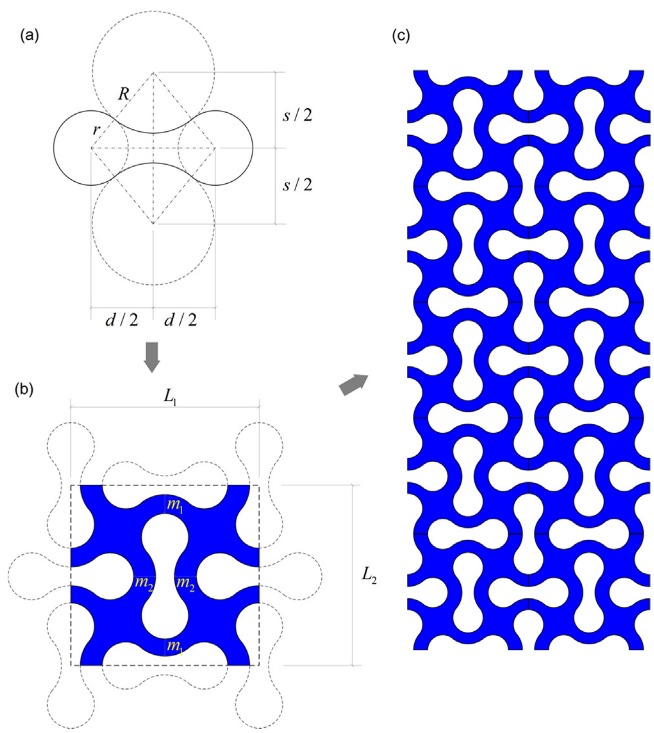

Fig. 2. Geometrical configuration of (a) the peanut-shaped hole, (b) the unit cell and (c) the lattice structure.

$$A = 2\pi r^2 + \frac{ds}{2} - 2R^2 \arcsin\left(\frac{d}{2(R+r)}\right) - 2r^2 \arccos\left(\frac{d}{2(R+r)}\right) \tag{4}$$

Accordingly, the equivalent density of such cellular structure can be written as

$$\frac{\rho^*}{\rho_s} = 1 - \phi \tag{5}$$

where ρ^* is the equivalent density of cellular material, and ρ_s is the density of base material.

Therefore, there are four primary design parameters for generating this symmetric unit cell microstructure with desired porosity, i.e. the unit cell size L, the small circle radius r, the large circle radius R, and

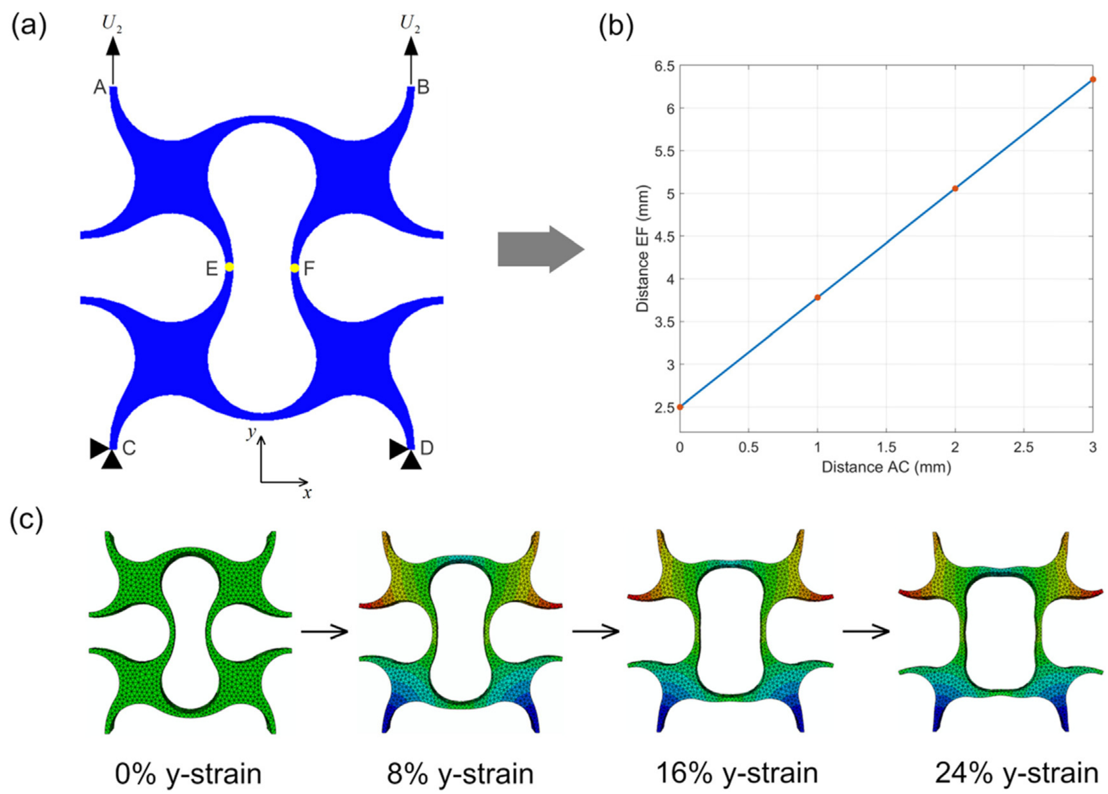

Fig. 3. (a) The unit cell under applied strain in the vertical direction, (b) the induced deformation in the horizontal direction and (c) the system shape at different strains.

the centroid-to-centroid distance d. The Poisson's ratio and porosity of the microstructure are a function of these essential parameters. Consequently, based on the well-designed unit cell, the lattice can be generated by a regular square pattern in the two directions. Fig. 2c shows a sample of unit cell array.

2.2. Deformation mechanism

To explore deformation mechanism of the unit cell proposed, the specific displacement U_2 shown in Fig. 3a is applied on the top surface of the unit cell for modeling the tensile behavior, whilst its bottom is fixed. The sample of unit cell is generated by setting $L = 12.5\,\text{mm}$, $r = 1.875\,\text{mm}$, $R = 4.025\,\text{mm}$ and $d = 6.25\,\text{mm}$. Fig. 3b illustrates the deformation results of the distance between Point E and F as the distances AC and BD increase. The unit cell is numerically studied using finite element methods [35–37]. The applied deformations are assumed to vary at 0%, 8%, 16% and 24% in the distances AC and BD, which respectively correspond to 0%, 8%, 16% and 24% tensile strains in the vertical direction, while the system becomes larger in the horizontal direction (i.e. the distance EF increases) as a result of an applied strain in the vertical direction. Hence, the system exhibits apparent negative Poisson's ratio. Furthermore, it is apparent that the existence of peanut-shaped holes divides the base material into four star-shaped solid parts which connect each other. The finite element simulation displays that the star-shaped solid parts rotate as the system is strained in the vertical direction. It is such rotation that makes the distance EF increases. Fig. 4 illustrates the deformation mechanism of the unit cell.

3. Characterization of mechanical properties

Having identified configuration for the metamaterial unit cell, we next study the detailed mechanical response through a combination of experiment and numerical simulation. All quasi-static uniaxial tensile tests are conducted in an SANS Electromechanical Universal Testing

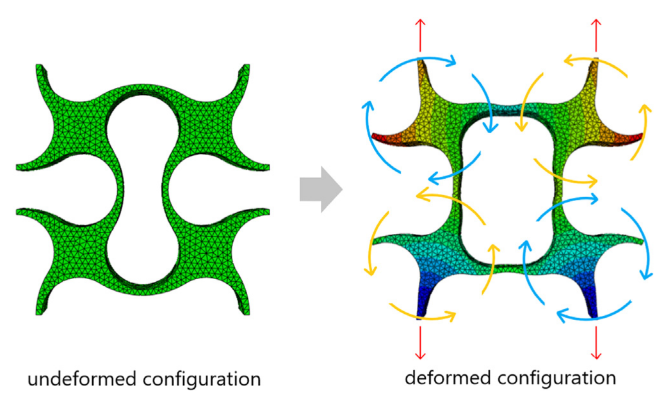

Fig. 4. Deformation mechanism of the unit cell.

System with a calibrated loading cell of 5KN, and the corresponding load resolution for this loading cell is 0.01 N. The samples are loaded via displacement control and the moving speed of upper cross-head is set as 0.05 mm/min, while the bottom cross-head is fixed. The remaining boundaries of the samples are traction free. Here, similarly to previous studies using optical system to monitor the deformation of cellular specimens [30,38], the caused strain within the samples are captured using a Imetrum Non-Contact Precision Measurement System, which can directly measure the distance change between the chosen reference points.

3.1. Experimental program

Firstly, a metamaterial specimen consisting of 4×8 unit cell array is fabricated and mechanically tested and each square unit cell has dimensions of $L = 20\,\text{mm}$, $r = 2.7\,\text{mm}$, $R = 7.2\,\text{mm}$, and $d = 10\,\text{mm}$. The corresponding porosity is 0.61 or 61%. The thickness of the unit cell is 4 mm. Using 3D printing technology, such specimen is fabricated from a

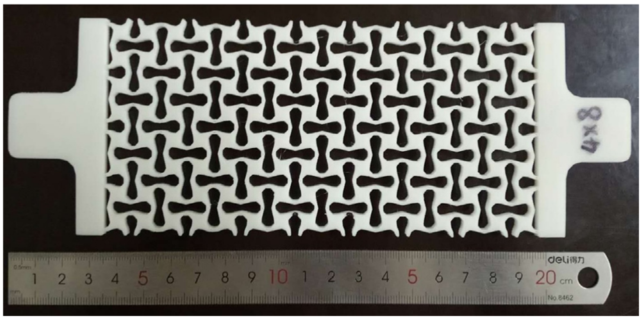

Fig. 5. The printed auxetic specimen with 4×8 cells.

raw polylactic acid (PLA) base material with elastic modulus $E_s = 3\text{GPa}$ and Poisson's ratio $\nu_s = 0.38$, which are determined through tensile tests following ASTM standards for 3D printed dog bone specimen. The printing machine is Wiiboox Company2 printer with printing resolution of 0.05 mm. Fig. 5 displays the printed auxetic specimen. The specimen is pulled by applying different static tensile displacements such as 1 mm, 1.5 mm, 2 mm, 2.5 mm, and 3 mm, respectively. The longitudinal and transverse deformation of the specimen is measured by tracking the four reference points (A, B, C, D) marked in black color on the specimen, which are chosen to keep far away to the loaded faces and outer boundaries to minimize the influence of boundary conditions, by the video extensometers purchased from Imetrum company (see Fig. 6). By recording the change of local distance of the two marked reference points, the local normal strain along the x and y directions can be then obtained as

$$\varepsilon_x = \frac{\Delta x - \Delta x_0}{\Delta x_0}, \quad \varepsilon_y = \frac{\Delta y - \Delta y_0}{\Delta y_0} \tag{6}$$

where Δx_0 and Δx are the initial and deformed distances between the reference points AD and BC, while Δy_0 and Δy denote the initial and deformed distances between the two reference points AB and DC. Here, the strain 1 and strain 2 represent the longitudinal normal strain in the y direction, and the strain 3 and strain 4 represent the transverse normal strain in the x direction, as shown in Fig. 6.

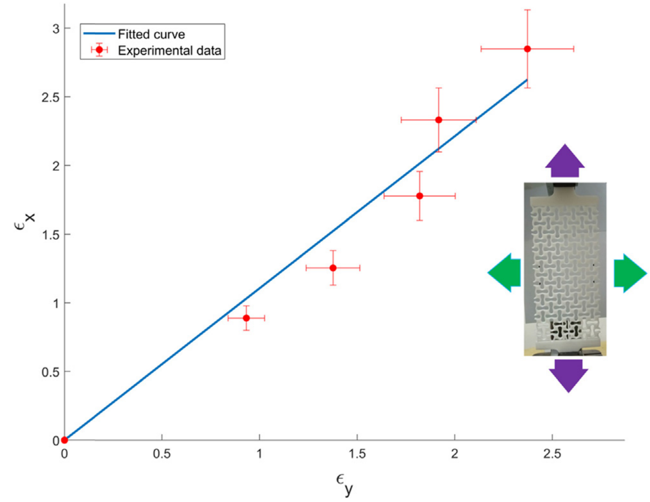

Fig. 7. Evolution of transverse strain for the metamaterial specimen.

Fig. 7 indicates the dependence of the transverse normal strain ε_x on the longitudinal strain ε_y. The error bars on the experimental points in Fig. 7 is set as 10% to the test value. Clearly, the data show that the transverse strain increases as the longitudinal tensile strain increases. This indicates that the structure expands in the lateral x direction orthogonal to the loaded y direction. To quantify this lateral effect, the Poisson's ratio is calculated from the averaged engineering strain as

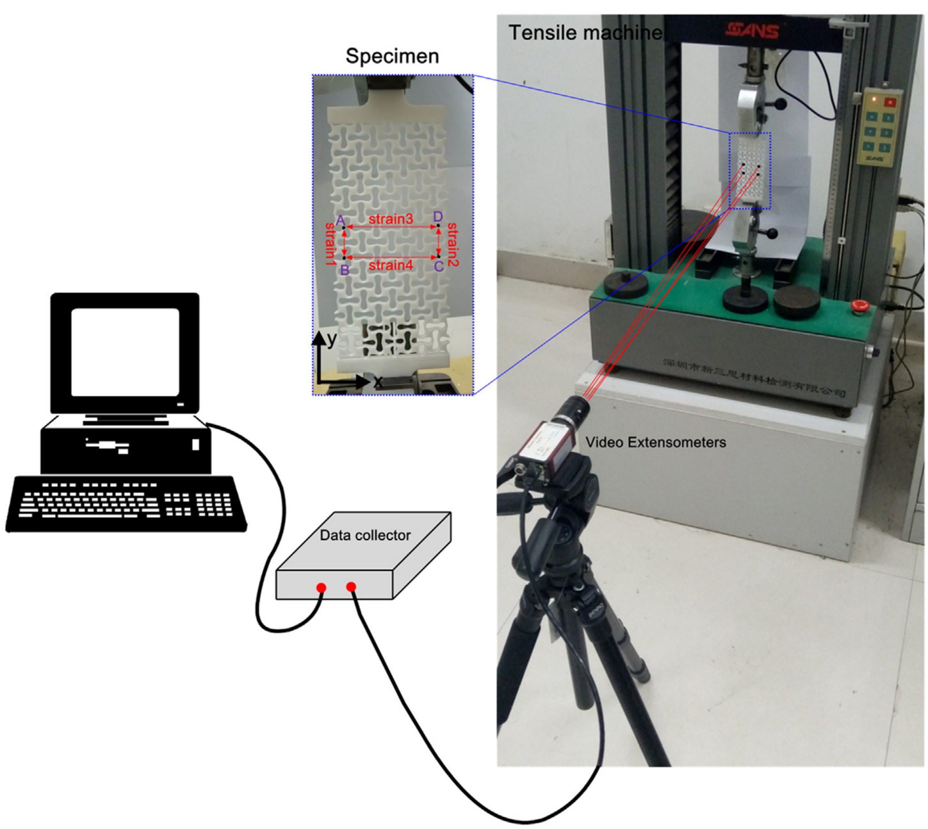

Fig. 6. Experimental setup of uniaxial tension for the printed metamaterial specimen.

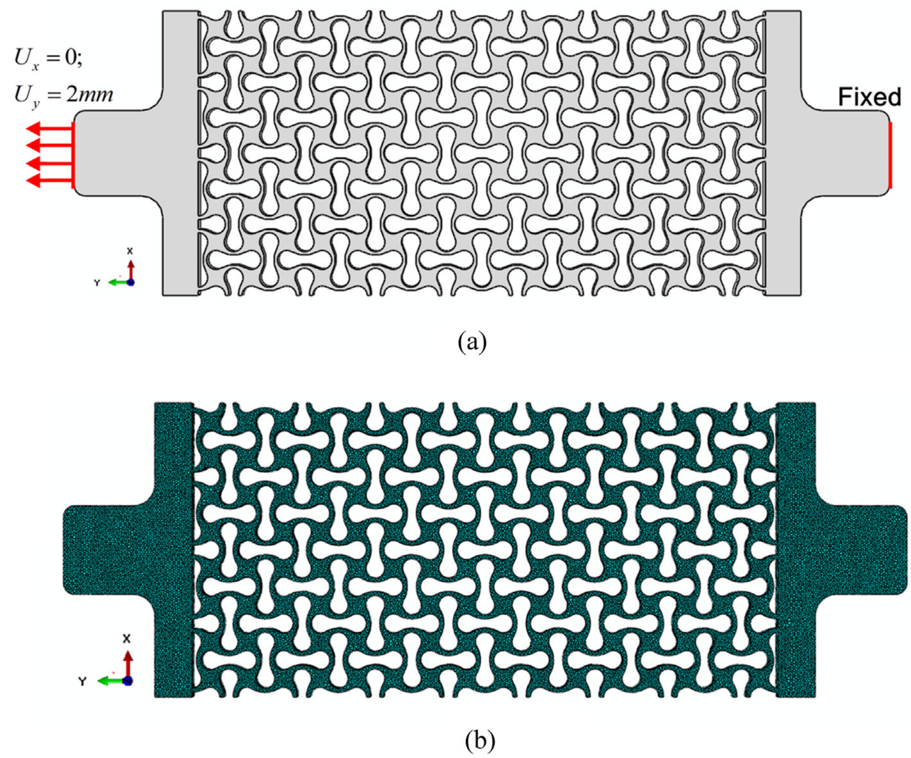

Fig. 8. (a) Finite element model of the specimen with 4 × 8 unit cell array and (b) mesh configuration.

$$\nu_{xy} = -\frac{\varepsilon_x}{\varepsilon_y} \tag{7}$$

which can be evaluated in practice by the slope of the fitting line to the experimental data given in Fig. 7. Here, the experimental result of Poisson's ratio for the specimen is −1.1066.

3.2. Finite element modeling

To verify the auxetic behavior measured in the experiment, the finite element simulation is performed for an auxetic structure as plotted in Fig. 8a. The quadratic finite element C3D10 with reduced integration provided in the commercial software ABAQUS is employed to model the structure, as shown in Fig. 8b. With the applied vertical displacement, the strain ε_x and ε_y can be calculated, and then the Poisson's ratio in the x direction can be determined by Eq. (7). Fig. 9 shows the deformation diagram in the x direction when 723,232 nodes and 44,865 elements are used to discretize the structure, and it is noticed that the structure remarkably expands in the x direction, under the applied displacement in the y direction. Moreover, the mesh convergence analysis is carried out because of the dependence of finite element accuracy on mesh density. Fig. 10 indicates the convergence curve of Poisson's ratio to the number of nodes. It is observed that when the number of nodes exceeds 326210, a convergent result can be reached. Here, in order to highly accurately predict the mechanical response of the structure near the holes, a refined mesh with 723,232 nodes is used. Correspondingly, the Poisson's ratio of the auxetic structure calculated by the finite element analysis is ν_{xy}= −1.1770, which has a relative error 6.36% to the experimental result. Clearly, a good agreement is observed between the simulation and experimental results. Therefore, the auxetic effect of the designed structure is demonstrated by both the experiment and the numerical simulation, and simultaneously the established finite element model is verified.

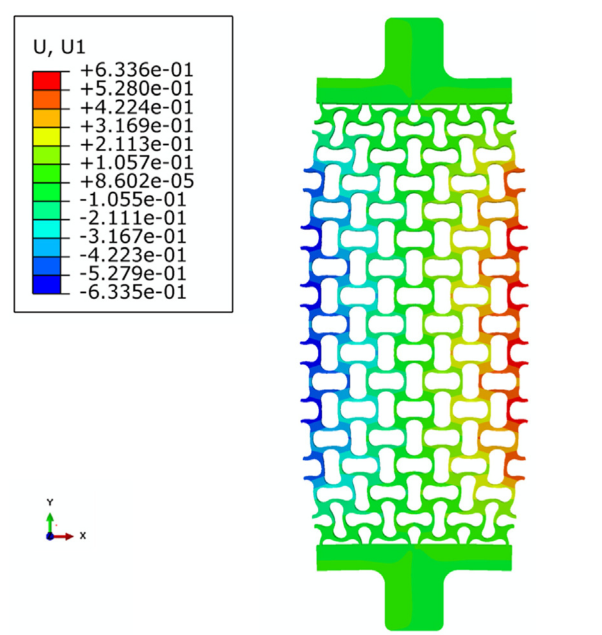

Fig. 9. Deformation calculation for the specimen with the applied displacement 1 mm in the y direction.

3.3. Comparison to the auxetic material with elliptical hole pattern

Except for the present structure with auxetic response, the pattern of mutually orthogonal ellipses was observed to generate auxetic response as well. Fig. 11 displays two kinds of auxetic structures with almost the same porosity of 66%. The structure a in Fig. 11 is designed with the dimensions of L = 20 mm, r = 3 mm, R = 4 mm, and d = 10 mm, while the structures b, c and d in Fig. 11 are designed by arranging mutually orthogonal elliptical holes with different semi-axes. In Fig. 11, the

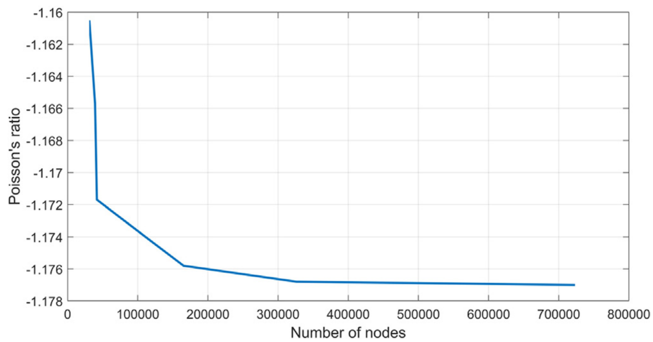

Fig. 10. Convergence analysis for different mesh densities.

structure b is designed that the elliptic holes have the major axis of 5.27 mm and the minor axis of 4 mm, the structure c is with the elliptic holes having the major axis 5.86 mm and the minor axis 3.6 mm, and the structure d contains the elliptic holes with their major axis of 6.59 mm and the minor axis of 3.2 mm. Making use of the finite element simulation, the corresponding Poisson's ratio is evaluated as −1.1276, −1.2979, −1.3988 and −1.3690 for the structures a, b, c and d, respectively. It indicates that the present auxetic structure can produce slightly larger negative Poisson's ratio than those produced by the structures b, c, and d under the almost same porosity. Besides, Fig. 11A, B, C and D respectively display the induced stress distribution in the structures a, b, c and d under the same tensile condition. It is clearly observed that the stress level of the present structure (as shown in Fig. 11a) is much smaller than those of the structures b, c, and d. The maximum Von-Mises stress is 4.53 MPa in the structure a, 29.6 MPa in the structure b, 19.6 MPa in the structure c and 11.01 MPa in the structure d, respectively. Obviously, the elliptical hole brings more significant stress concentration than the peanut-shaped hole. Such stress concentration is not beneficial to practical applications.

3.4. Parametric study

Through the experiment and numerical analysis implemented above, it is clear that the structure presented in this paper has distinctive auxetic characterization, due to the rotation effect of solid parts at the four corners. Moreover, as indicated in Section 2.1, there are four essential parameters (L, r, R and d) for determining the geometrical configuration of unit cell. To further understand the auxetic behavior of the present structure, a comprehensive study on the effect of these important geometrical parameters on the negative Poisson's ratio is performed in this section.

3.4.1. Effect of unit cell size

The geometrical configuration of structure may change in terms of the given size of unit cell, when the length and width of specimen are fixed. In order to investigate the effect of unit cell size on the Poisson's ratio, a series of finite element models with different unit cell sizes are built as shown in Fig. 12. For the model with structure configuration of 2×4 cell array, each unit cell has the dimensions of $L = 40$ mm, $r = 6$ mm, $R = 9.96$ mm, $d = 20$ mm. For the other models, the sizes of unit cell are given by shrinking the reference unit cell in the 2×4 cell array structure in integer divide. That is, for the structure configurations with 4×8, 8×16 and 10×20 cell arrays, the shrinking rate is 2, 4 and 5, respectively. For such case, the porosity keeps 0.69 unchanged. The variations of Poisson's ratio are listed in Table 1. It's clear that all values of Poisson's ratios are negative and the absolute value decreases as the unit cell becomes smaller. This is because that the deformation of smaller unit cells caused by internal rotation is getting weaker whilst pulling equally.

3.4.2. Effect of circle radius contrast

The ratio of R/r obviously influences the geometrical configuration of the present auxetic structure. Here, a series of numerical models with same dimensions of 40 mm × 80 mm but different R/r ($R/r = \frac{4}{3}, \frac{5}{3}, \frac{6}{3}, \frac{7}{3}$) are established in which the other geometrical parameters of the unit cell are kept unchanged as $L = 20$ mm, $r = 3$ mm,

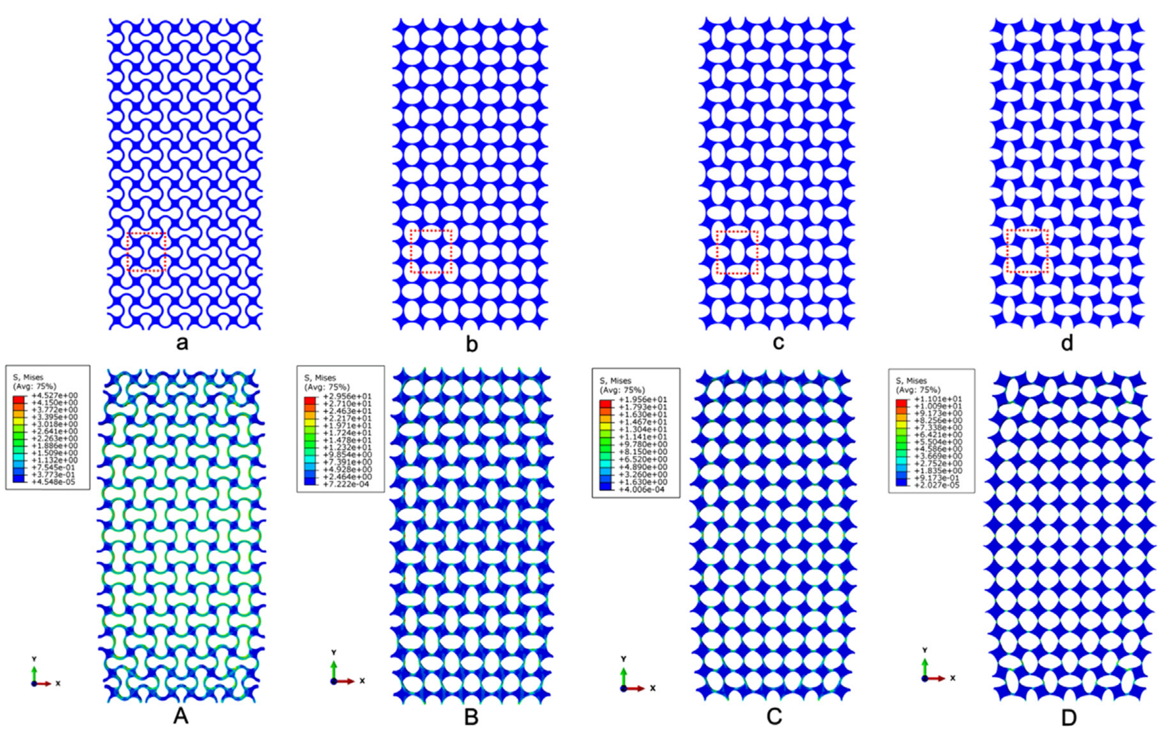

Fig. 11. Samples with different patterns of mutually orthogonal peanut-shaped holes (a) and elliptic holes (b, c and d), and the corresponding stress results for peanut-shaped holes (A) and elliptic holes (B, C and D).

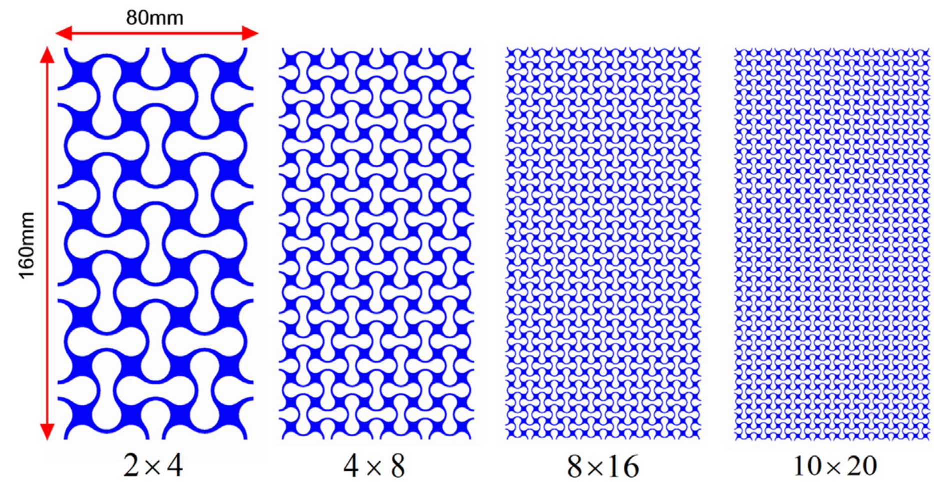

Fig. 12. Samples with same size and different unit cell patterns.

Table 1
The variations of Poisson's ratio with different unit cell patterns.

Configuration	2 × 4	4 × 8	8 × 16	10 × 20
ϕ	0.69	0.69	0.69	0.69
ν_{xy}	−1.6473	−1.1857	−1.0277	−1.0036

Table 2
Variations of Poisson's ratio for different R/r.

R/r	4/3	5/3	6/3	7/3
ϕ	0.66	0.69	0.71	0.73
ν_{xy}	−1.1274	−1.1816	−1.2136	−1.2247

$d = 10$ mm. The models are displayed in Fig. 13. Table 2 shows the values of Poisson's ratio and porosity of the models, from which it is observed that the ratio R/r significantly influences the negative Poisson's ratio of the material and its value almost decreases with respect to R/r linearly. Correspondingly, the porosity increases with respect to R/r. The reason is that the length m becomes shorter as the ratio R/r increases. As a result, the extent of internal rotation in the unit cell becomes wider.

3.4.3. Effect of the centroid-to-centroid distance

In addition to the size of unit cell and the ratio of circle radius studied above, the centroid-to-centroid distance d denoted by O_1O_2 (see Fig. 14) also affects the structure configuration. In this investigation, a series of unit cells with different distance O_1O_2 are designed to form different auxetic structures which have the same size of unit cells (4 × 8). The unit cell has the same dimensions of $L = 20$ mm, $r = 3$ mm, $R = 7.4$ mm but different centroid-to-centroid distance d varying from 8 mm to 9.2 mm. The results listed in Table 3 reveal the porosity slowly increases with the increase of d and the negative Poisson's ratio effect of the material becomes slightly stronger with the bigger d. The reason is that, when the centroid-to-centroid distance d increases, the length m in the unit cell becomes shorter, thus the connection strength of neighboring solids becomes weaker.

3.4.4. Effect of base material

In this part, the effect of base material is investigated. To this end, consider the structure configuration with 4 × 8 array in which each unit cell has the dimensions of $L = 20$ mm, $r = 3$ mm, $R = 4$ mm, and $d = 10$ mm, as shown in Fig. 15. In order to study the influence of the base material with elastic modulus E_s, the elastic modulus E_s is changed from 0.5 GPa to 70 GPa, while the Poisson's ratio ν_s of the base material is kept unchanged in 0.38. On the other hand, to study the influence of Poisson's ratio of the base material, the Poisson's ratio ν_s is set to be changed from 0.1 to 0.4, while the elastic modulus E_s of the base material takes 3GPa. From Tables 4 and 5, it is found that the negative Poisson's ratio ν_{xy} of the auxetic structure is insensitive to the elastic modulus E_s and Poisson's ratio ν_s. Therefore, it can be concluded that the negative Poisson's ratio is independent on the choice of base

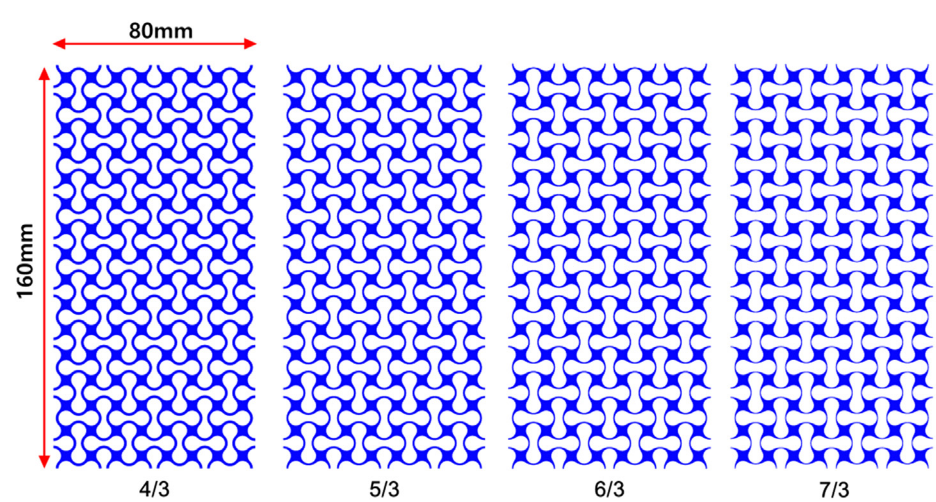

Fig. 13. Models with different R/r.

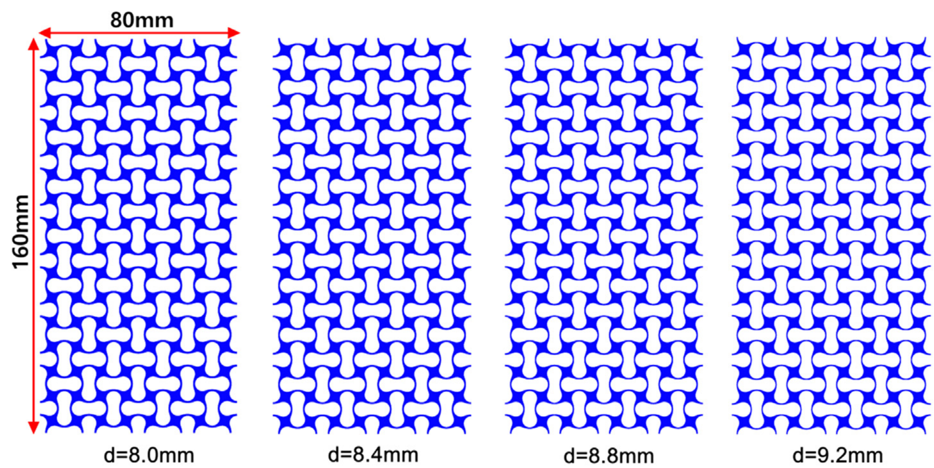

Fig. 14. Unit cells with different centroid-to-centroid distance d.

Table 3
Variations of Poisson's ratio for different centroid-to-centroid distance.

d (mm)	8.0	8.4	8.8	9.2
ϕ	0.69	0.70	0.71	0.72
ν_{xy}	−1.2167	−1.2269	−1.2295	−1.2306

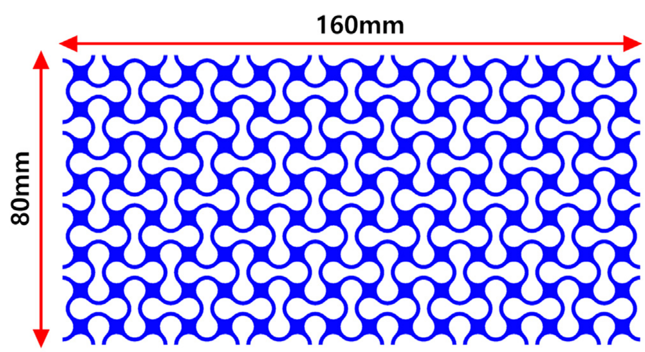

Fig. 15. Auxetic model with 4 × 8 array with unit cell size 20 mm

Table 4
The effect of elastic modulus of the base material.

E_s (GPa)	0.5	5	50	70
ν_{xy}	−1.1274	−1.1274	−1.1274	−1.1274

Table 5
The effect of Poisson's ratio of the base material.

ν_s	0.1	0.2	0.3	0.4
ν_{xy}	−1.1274	−1.1274	−1.1274	−1.1274

material.

4. Conclusions

In the study, a new two-dimensional mechanical metamaterial showing apparent auxetic effect is designed, fabricated and experimentally characterized. Meanwhile, the finite element simulation on auxetic behavior of the metamaterial is carried out. A good agreement of Poisson's ratio of the present auxetic material is observed between the numerical and experimental predictions. Furthermore, the effects of some essential parameters controlling auxetic performance of the material are investigated numerically. The conclusions are drawn from the results as follows: (1) a new way to design 2D auxetic material with controllable porosity is demonstrated by introducing peanut-shaped holes, which can produce larger negative Poisson's ratio and achieve lower stress level than elliptical holes; (2) the smaller size of unit cell causes the larger negative Poisson's ratio for this auxetic material under certain length and width of the auxetic material, although the porosity keeps unchanged; (3) the parameters R/r and d show similar effect on the negative Poisson's ratio of auxetic material, because they both influence the length m of ligament separating neighboring holes; (4) the effects of elastic properties of base material on the negative Poisson's ratio of auxetic material can be neglected.

In summary, the auxetic behavior of the present design is fully controlled by the geometrical parameters which alter the microstructure of unit cell. Therefore, this work provides not only a guide for the new design of auxetic materials but also a basis for future optimized investigations of these parameters.

CRediT authorship contribution statement

Hui Wang: Conceptualization, Methodology, Writing - original draft, Writing - review & editing, Supervision. **Yuxuan Zhang:** Data curation, Formal analysis, Resources, Validation, Writing - original draft. **Wanqing Lin:** Formal analysis, Resources, Validation. **Qing-Hua Qin:** Writing - review & editing, Supervision.

Acknowledgments

The work described in this paper was supported by the Program for Innovative Research Team of Science & Technology of Henan Province of China (Grant no. 19IRTSTHN020) and the National Natural Science Foundation of China (No. 11772204).

Data availability

The raw/processed data required to reproduce these findings cannot be shared at this time as the data also forms part of an ongoing study.

References

[1] Z.G. Nicolaou, A.E. Motter, Mechanical metamaterials with negative compressibility transitions, Nat. Mater. 11 (2012) 608–613.
[2] S. Agarwal, Y.K. Prajapati, Multifunctional metamaterial surface for absorbing and sensing applications, Opt. Commun. 439 (2019) 304–307.
[3] K. Cai, J. Luo, Y. Ling, J. Wan, Q.H. Qin, Effects of size and surface on the auxetic behaviour of monolayer graphene kirigami, Sci. Rep. 6 (2016) 35157.
[4] J.N. Grima, R. Gatt, Perforated sheets exhibiting negative Poisson's ratios, Adv. Eng. Mater. 12 (2010) 460–464.
[5] R. Lakes, Deformation mechanisms in negative Poisson's ratio materials, J. Mater.

Sci. 26 (1991) 2287–2296.
[6] J.N. Grima, R. Gatt, N. Ravirala, A. Alderson, K.E. Evans, Negative Poisson's ratios in cellular foam materials, Mater. Sci. Eng. A 423 (2006) 214–218.
[7] N. Liu, M. Becton, L. Zhang, K. Tang, X. Wang, Mechanical anisotropy of two-dimensional metamaterials: a computational study, Nanoscale Adv. 1 (2019) 2891–2900.
[8] P.S. Theocaris, G.E. Stavroulakis, P.D. Panagiotopoulos, Negative Poisson's ratios in composites with star-shaped inclusions, Int. J. Appl. Mech. 67 (1997) 274–286.
[9] A. Bacigalupo, L. Gambarotta, Homogenization of periodic hexa- and tetrachiral cellular solids, Compos. Struct. 116 (2014) 461–476.
[10] H.M.A. Kolken, A.A. Zadpoor, Auxetic mechanical metamaterials, RSC Adv. 7 (2017) 5111–5129.
[11] J. Schwerdtfeger, F. Wein, G. Leugering, R.F. Singer, C. Körner, M. Stingl, F. Schury, Design of auxetic structures via mathematical optimization, Adv. Mater. 23 (2011) 2650–2654.
[12] L. Wang, C. Wang, Negative/zero thermal expansion in black phosphorus nanotubes, Phys. Chem. Chem. Phys. 20 (2018) 28726–28731.
[13] V. Oddone, R.C. Wimpory, S. Reich, Understanding the negative thermal expansion in planar graphite-metal composites, J. Mater. Sci. 54 (2019) 1267–1274.
[14] Y. Zhao, J. Su, Cloaking magnetic field and generating electric field with topological insulator and high permeability material, Chin. J. Phys. 57 (2019) 14–20.
[15] C. Gustavo Mendez, J. Manuel Podesta, O. Lloberas Valls, S. Toro, A. Edmundo Huespe, J. Oliver, Computational material design for acoustic cloaking, Int. J. Numer. Meth. Eng. 112 (2017) 1353–1380.
[16] X. Yu, Z. Lu, T. Liu, L. Cheng, J. Zhu, F. Cui, Sound transmission through a periodic acoustic metamaterial grating, J. Sound Vib. 449 (2019) 140–156.
[17] M.H. Lu, L. Feng, Y.F. Chen, Phononic crystals and acoustic metamaterials, Mater. Today 12 (2009) 34–42.
[18] D. Schneider, N. Gomopoulos, C.Y. Koh, P. Papadopoulos, F. Kremer, Edwin L. Thomas, G. Fytas, Nonlinear control of high-frequency phonons in spider silk, Nat. Mater. 15 (2016) 1079–1083.
[19] H. Singh, B.S. Sohi, A. Gupta, Designing and analysis of cross-shaped CRLH metamaterial for wide band negative index characteristics, Mater. Res. Express 6 (2019).
[20] T. Frenzel, M. Kadic, M. Wegener, Three-dimension mechanical metamaterials with a twist, Science 358 (2017) 1072–1074.
[21] B.B. Zheng, R.C. Zhong, X. Chen, M.H. Fu, L.L. Hu, A novel metamaterial with tension-torsion coupling effect, Mater. Design 171 (2019) 107700.
[22] A. Casalotti, S. El-Borgi, W. Lacarbonara, Metamaterial beam with embedded nonlinear vibration absorbers, Int. J. Nonlin. Mech. 98 (2018) 32–42.
[23] M. Nouh, O. Aldraihem, A. Baz, Wave propagation in metamaterial plates with periodic local resonances, J. Sound Vib. 341 (2015) 53–73.
[24] X. Ren, R. Das, P. Tran, T.D. Ngo, Y.M. Xie, Auxetic metamaterials and structures: a review, Smart Mater. Struct. 27 (2018) 023001.
[25] R.H. Baughman, J.M. Shacklette, A.A. Zakhidov, S. Stafstrom, Negative Poisson's ratios as a common feature of cubic metals, Nature 392 (1998) 362–365.
[26] F. Scarpa, G. Tomlinson, Theoretical characteristics of the vibration of sandwich plates with in-plane negative Poisson's ratio values, J. Sound. Vib. 230 (2000) 45–67.
[27] J. Dirrenberger, S. Forest, D. Jeulin, Effective elastic properties of auxetic microstructures: anisotropy and structural applications, Int. J. Mech. Mater. Des. 9 (2013) 21–33.
[28] H.W. Tang, W.D. Chou, L.W. Chen, Wave propagation in the polymer-filled star-shaped honeycomb periodic structure, Appl. Phys. A-Mater. 123 (2017) 523.
[29] W. Chen, X. Tian, R. Gao, S. Liu, A low porosity perforated mechanical metamaterial with negative Poisson's ratio and band gaps, Smart Mater. Struct. 27 (2018) 115010.
[30] C. Ma, H. Lei, J. Liang, W. Wua, T. Wang, D. Fang, Macroscopic mechanical response of chiral-type cylindrical metastructures under axial compression loading, Mater. Design 158 (2018) 198–212.
[31] M.L.D. Bellis, A. Bacigalupo, Auxetic behavior and acoustic properties of microstructured piezoelectric strain sensors, Smart Mater. Struct. 26 (2017) 0964–1726.
[32] K. Meena, S. Singamneni, A new auxetic structure with significantly reduced stress concentration effects, Mater. Design 173 (2019) 107779.
[33] X. Ren, J.H. Shen, A. Ghaedizadeh, H.Q. Tian, Y.M. Xie, A simple auxetic tubular structure with tuneable mechanical properties, Smart Mater. Struct. 25 (2016) 065012.
[34] X. Ren, J. Shen, P. Tran, T.D. Ngo, Y.M. Xie, Design and characterisation of a tuneable 3D buckling-induced auxetic metamaterial, Mater. Design 139 (2018) 336–342.
[35] O.C. Zienkiewicz, R.L. Taylor, The Finite Element Method for Solid and Structural Mechanics, Elsevier, 2005.
[36] Q.H. Qin, Trefftz finite element method and its applications, Appl. Mech. Rev. 58 (2005) 316–337.
[37] H. Wang, Q.H. Qin, Fundamental-solution-based hybrid FEM for plane elasticity with special elements, Comput. Mech. 48 (2011) 515–528.
[38] M. Taylor, L. Francesconi, M. Gerendas, A. Shanian, C. Carson, K. Bertoldi, Low porosity metallic periodic structures with negative Poisson's ratio, Adv. Mater. 26 (2014) 2365–2370.